

Aerosol optical properties during dust and biomass episodes

C. Shi et al.

This discussion paper is/has been under review for the journal Atmospheric Measurement Techniques (AMT). Please refer to the corresponding final paper in AMT if available.

Aerosol optical properties during dust and biomass burning episodes retrieved from sun-photometer over Shanghai

C. Shi¹, S. Wang^{1,3}, R. Zhou¹, D. Li², H. Zhao¹, R. Liu¹, Z. Li², and B. Zhou¹

¹Shanghai Key Laboratory of Atmospheric Particle Pollution and Prevention (LAP³), Department of Environmental Science and Engineering, Fudan University, Shanghai 200433, China

²State Environmental Protection Key laboratory of Satellites Remote Sensing, Institute of Remote Sensing and Digital Earth of Chinese Academy of Sciences, Beijing 100049, China

³School of Environment and Architecture, University of Shanghai for Science and Technology, Shanghai 200093, China

Received: 10 November 2013 – Accepted: 2 December 2013 – Published: 17 December 2013

Correspondence to: B. Zhou (binzhou@fudan.edu.cn)

Published by Copernicus Publications on behalf of the European Geosciences Union.

Title Page

Abstract

Introduction

Conclusions

References

Tables

Figures

⏪

⏩

◀

▶

Back

Close

Full Screen / Esc

Printer-friendly Version

Interactive Discussion

Abstract

Ground-based observation over Shanghai was carried out from 28 March to 25 June 2013 in an urban site at Fudan University (31°18' N, 121°29' E). Utilizing a sun/sky radiometer (CE318), aerosol properties including thickness, scattering, asymmetry, and particle size distribution were inverted for two types (dust and biomass burning). Dust aerosol showed large optical depth (AOD at 440 nm \sim 1.06) with small value of Ångström parameter (α) around 0.74, indicating the strong optical extinction capability of large-size particles. Aerosol loading (\sim 0.72 at 440 nm) was discovered to be coupled with large α ($>$ 1.05) for biomass smoke. The particle size distribution was dominated by the coarse mode for dust with high concentration ratio between coarse and fine mode ($V_C/V_F \sim$ 3.76). Biomass burning particle primarily accumulated around 0.17 μ m and performed smaller V_C/V_F (\sim 0.99). Aerosol in fine mode mainly accounted for the optical extinction process in Shanghai as its volume concentration was well-correlated with AOD ($R \sim$ 0.88 in average condition). The value of single scattering albedo (SSA) during agricultural residue burning displayed variation from 0.902 to 0.922 with a descending trend at 670–1020 nm while SSA increased at all wavelengths for dust aerosol. The negative correlation between SSA \cdot AOD and α was analyzed to capture the order of scattering capability: urban/industrial $<$ biomass $<$ dust aerosol. Higher value of asymmetry factor at 1020 nm (\sim 0.652) of dust aerosol was found compared to average condition and biomass smoke (both were equal to 0.625), imposing the enhanced forward scattering of dust particles in NIR band. The validation of AOD vs. MODIS showed errors in dust and biomass samples, which may be attributed to the variable SSA in YRD. The ascending deviation also existed in clear condition, which could be caused by the overestimation of ground reflectance in MODIS algorithm.

Aerosol optical properties during dust and biomass episodes

C. Shi et al.

Title Page

Abstract

Introduction

Conclusions

References

Tables

Figures



Back

Close

Full Screen / Esc

Printer-friendly Version

Interactive Discussion



1 Introduction

More than 30 yr witnessed the rapid economic growth in China with prosperous industrialization and urbanization, generating various anthropogenic emissions and consequently deteriorating the air quality (Lei et al., 2011; Lu et al., 2011; Westerdahl et al., 2009), descending the air visibility (Jinhuan and Liquan, 2000; Zhang et al., 2011) while increasing aerosol loadings (He et al., 2012a; Xue et al., 2011). Aerosol impacts considerably and plays the key role in global climate change by affecting the radiation energy budget with corresponding uncertainty (Badarinath et al., 2007; Metz et al., 2007; Quaas et al., 2008). Indirectly, aerosol can also participate in the formation process of clouds as condensation nuclei, exerting influences on cloud cover and precipitation distribution (Ramanathan et al., 2001). The optical properties of aerosol serve as a major factor affecting radiative forcing in the performance of scattering and absorption process (Haywood and Boucher, 2000; Jacobson, 2001; Takemura et al., 2002). Studies on climate changes were conducted intensively using aerosol models with parameterized indices including single scattering albedo (SSA) and asymmetry factor (ASY) in numerical simulation (Mugnai and Wiscombe, 1986; Russell et al., 1999; Takemura et al., 2002). Among these radiatively important parameters, SSA was indispensable in estimating ground albedo in remote sensing retrievals while the biggest challenge existed in distinguishing aerosol types (Chu et al., 2003; Kaufman et al., 2001). Aerosols from different sources can be classified into distinctive types with dynamic variations in optical characteristics (Dubovik et al., 2002; Eck et al., 2005). For these aerosols with diverse types, the chemical composition along with hygroscopic growth capability were discovered to be main factors determining optical properties (Eck et al., 2005; Kim et al., 2006). Continental aerosol was found to be mainly constituted with mineral dust, carbonaceous particles from biomass burnings (including agriculture residue and forest fire) as well as marine particles and secondary aerosol (Badarinath et al., 2011; Limbeck et al., 2003; Tsunogai et al., 1985). Due to the microphysical properties of

Aerosol optical properties during dust and biomass episodes

C. Shi et al.

Title Page

Abstract

Introduction

Conclusions

References

Tables

Figures



Back

Close

Full Screen / Esc

Printer-friendly Version

Interactive Discussion

aerosol present temporal and spatial variability, it is essential to do specific observation on respective aerosol type in different regions (Dubovik et al., 2002).

Yangtze River Delta (YRD) is located in the East China with fast economic development in recent decades, during which aerosol loading was lifted up acutely (He et al., 2012a). As the most populated city cluster in China (with the population more than 150 million till the year of 2011), mixed types of aerosols such as industrial/urban, dust, sea salt and smoke particles were discovered in the boundary layer by abundant studies (Fu et al., 2008; Gao et al., 2009; He et al., 2010; Huang et al., 2011). The Chinese Sun Hazemeter Network (CSHNET) operated a nationwide observation finding that the aerosol optical properties in Eastern China behaved as mixtures of mineral particles, smoke and anthropogenic pollutant (Xin et al., 2005). Distinctive from the aerosol characteristics in northern China, whose seasonal variations were obvious, airborne aerosol loading exhibited daily fluctuations dynamically in contrast to the dimming seasonal changes in YRD (Wang et al., 2006). Investigated and inversed with sun-photometer by Xia et al. (2007), the notable aerosol direct radiative forcing (annually mean surface shortwave radiation and photosynthetically active radiation were computed as -38.4 W m^{-2} and -17.8 W m^{-2} respectively) by burdened aerosol loadings was calculated out in Taihu area. Shanghai, the biggest megacity in China, is suited in eastern YRD district and facing East China Sea. The coastal location makes the chemical composition and formation mechanism of aerosol here quite complicated, where sulfate, ammonium, black carbon (BC), mineral and marine can be measured (Li et al., 2010; Wang et al., 2000; Wang et al., 2006; Yang et al., 2009; Ye et al., 2003). So it is of considerable challenge to observe aerosol of single type in this metropolitan (Wang et al., 2009). According to relevant meteorology records of Shanghai, dust storms always invade in Spring through long-range transport and biomass burnings occur in June, July and August after summer harvest. During the air pollution episodes caused by mineral dust and biomass smoke, these two types of aerosols could be predominant pollutants in the ambient air, offering us an unprecedented opportunity to study their microphysical and chemical properties (Fan et al., 2010; Fu et al., 2010;

Aerosol optical properties during dust and biomass episodes

C. Shi et al.

Title Page

Abstract

Introduction

Conclusions

References

Tables

Figures

⏪

⏩

◀

▶

Back

Close

Full Screen / Esc

Printer-friendly Version

Interactive Discussion



Aerosol optical properties during dust and biomass episodes

C. Shi et al.

Title Page

Abstract

Introduction

Conclusions

References

Tables

Figures

⏪

⏩

◀

▶

Back

Close

Full Screen / Esc

Printer-friendly Version

Interactive Discussion

Wang et al., 2012a; Wang et al., 2009). Researches have adequately indicated the significance of both dust and crop residue burning aerosol in radiation process and climate responses (Shindell and Faluvegi, 2009; Takemura et al., 2005). China Aerosol Remote Sensing Network (CASNET) conducted an overall observation in YRD including two sites in Shanghai, revealing the different contribution of marine and inland aerosols in this coastal city (Pan et al., 2010). Apart from that, urban/industrial aerosol, which mainly consist of insoluble, soluble and soot species, is of broad existence in observation (Hess et al., 1998). Urban aerosols optical properties change with temperature, humidity, solar radiation intensity, altitude, wind speed and displays inhomogeneous distribution in different regions worldwide (Eck et al., 1999). Applying sun photometer with SKYRAD algorithm for retrievals, He et al. (2012b) presented the seasonal variations of optical properties in Shanghai. Their studies demonstrated the very effect of dust and biomass smoke aerosol on optical and radiative characteristics but they were absent from doing a respective analysis on aerosols of different types. Even if a certain type of aerosol is in dominance at one location, variability still behaves dynamically thanks to the meteorological conditions (Dubovik et al., 2002; Kim et al., 2004).

Using the observational data from 28 March to 25 June in 2013, this study aims to perform a comparative investigation on aerosol optical properties during spring dust and summer biomass burning episodes over Shanghai. Aerosol optical parameters (including optical depth, size distribution, volume concentration, single scattering albedo and asymmetry factors) were inverted by the optimized algorithm based on the classic one introduced by Dubovik and King (2000). Comparisons between the characteristics of these two types aerosols can serve to better understanding the regional aerosol microphysical and radiative features. The comprehensive learning about the respective type of aerosol should also be an indicator of building precise aerosol models and making revisions for the retrieval scheme. Finally, validations of MODIS AOD products with our ground-based observation results were presented to further discuss the inversion error and optimize the retrieval algorithm.

Aerosol optical properties during dust and biomass episodes

C. Shi et al.

Title Page

Abstract

Introduction

Conclusions

References

Tables

Figures

◀

▶

◀

▶

Back

Close

Full Screen / Esc

Printer-friendly Version

Interactive Discussion



Hutron Environment Technology Co., Ltd) automatic weather station, just 5 m away from sun-photometer. The data of AQI (Air Quality Index) and mass concentration of PM_{10} , $PM_{2.5}$, CO were all downloaded from Shanghai Environmental Monitoring Center (SEMC) website (<http://www.semc.com.cn>). AOD at 550 nm was also derived from MODIS (MODerate resolution Image Spectrometer) onboard Terra launched by NASA (<http://ladsweb.nascom.nasa.gov>). We choose the Collection 051 products to make validations with results from ground-based measurement.

2.2 Inversion algorithm and data description

The aerosol inversion algorithm put forward by Dubovik et al. (2000) and developed afterwards (Dubovik et al., 2002, 2006; Holben et al., 2006) was widely applied in AERONET (AERosol RObotic NETwork) established by NASA. Based on the code of this algorithm, two parts were optimized in this study, which differed itself from AERONET operational algorithm. One improvement for the classic algorithm was that a gain-corrected solid angle was introduced to produce interconverting calibrations coefficients during direct solar irradiance and diffuse-sky radiance measurement (Li et al., 2008). The core of radiance calibration transfer was to realize the refreshment of calibration coefficients on basis of radiometric characteristics of CE318. This alternative calibration method has been applied in CARSNET sky measurement in some observation sites (Che et al., 2009). The algorithm takes advantage of the direct-sun irradiance $E(\lambda)$ and diffused-sky radiance $L(\lambda)$ and defines a parameter Ω_v as their ratio:

$$\Omega_v = \frac{E(\lambda)}{L(\lambda)} = \frac{C_s(\lambda)V_s(\lambda)}{C_a(\lambda)V_a(\lambda)} \quad (1)$$

where $C(\lambda)$ and $V(\lambda)$ denote the calibration coefficients and the output DN of CE318 while the subscript s and a are short for sun irradiance and aureole sky radiance. Then the gain-corrected solid angle Ω , which is independent of wavelength, is needed

instead of Ω_v in the calibration transfer:

$$\Omega = \Omega_v(\text{HG}_a/\text{LG}) \quad (2)$$

where HG_a and LG are the fixed instrument internal electronic gains (this means the gains only depend on instrument). The calibration transfer performs a comparable accuracy using Ω with laboratory calibration coefficients (e.g. 3–5%). It's well-used to calibrate sky radiance from sun irradiance and could serve to recalibrate the historical measurements.

One of the largest error sources in retrieval is often related with ground reflectance. Li et al. (2006) used the 72 month averaged ground albedo (error ~ 10%) derived from MODIS to revise the reflectance parameter of the surface, which was also carried out in our retrieval. Additionally, the triplet direct-sun irradiance and almucantar measurement which is similar with AERONET serve to cloud-screening for all parameters. Then we introduce the radiatively important parameters in this study respectively.

AOD can be directly computed through the solar irradiance with Beer-Lambert law reproduced in Eq. (3), where τ is equal to the total scattering and absorption effects (k_{ex} as the extinction coefficient) in the atmosphere column. And the Ångström exponent (α) is calculated from 440 nm and 870 nm (nominal) wavelength in the Eq. (4), where β is the AOD at 1 μm (Ångström, 1964).

$$\tau = \int_0^I k_{\text{ext}} dI \quad (3)$$

$$\tau(\lambda) = \beta \lambda^{-\alpha} \quad (4)$$

The single scattering albedo is defined as the ratio between scattering coefficient (k_{scat}) with total extinction coefficient (k_{ext} , sum of scattering and absorption). It can be calculated by establishing a relationship between the actual and the estimated radiation

Aerosol optical properties during dust and biomass episodes

C. Shi et al.

Title Page

Abstract

Introduction

Conclusions

References

Tables

Figures

◀

▶

◀

▶

Back

Close

Full Screen / Esc

Printer-friendly Version

Interactive Discussion

parameters after cloud screening and quality control (Li et al., 2004).

$$\omega = \frac{k_{\text{scat}}}{k_{\text{ext}}} = \frac{k_{\text{scat}}}{k_{\text{scat}} + k_{\text{abs}}} \quad (5)$$

Phase functions $p(\Theta)$ are derived from total sky radiance and give rise to size distribution, refractive index, single scattering albedo (ω) of aerosol.

$$2\omega = \int_0^\pi \omega p(\Theta) \sin(\Theta) d\Theta \quad (6)$$

The optimized bimodal log-normal algorithm was applied universally in YRD (He et al., 2012b; Xia et al., 2007). As described in the Eq. (7), where $\frac{dV}{d\ln r}$ ($\mu\text{m}^3 \mu\text{m}^{-2}$) represents the size distribution, c_i is the column volume concentration r denotes the aerosol radius and r_{mean} is equal to the averages, σ is the standard deviation. The retrieval products provide 22 radius ranges from 0.05 to 15 μm in our study.

$$\frac{dV}{dr} = \sum_{i=1}^2 \frac{c_i}{r\sigma_i\sqrt{2\pi}} \exp\left(-\left(\frac{\ln(r/r_{\text{mean},i})}{2\sigma_i^2}\right)^2\right) \quad (7)$$

Usually, some certain single-valued representations of the angular scattering including the asymmetry parameter (g), the up-scatter fraction (b) were used to describe the distribution of scattering (Andrews et al., 2006). In the algorithm, g was computed from scattering angle(Θ) and phase function $p(\Theta)$ in diffuse-sky radiance:

$$g = \langle \cos \Theta \rangle = \frac{1}{2} \int_{-1}^{+1} p(\Theta) \cos \Theta d(\cos \Theta) \quad (8)$$

As sun-photometer ceased to work in rainy days and the inverted production quality was not guaranteed in too cloudy condition, the available samples in our observation

Aerosol optical properties during dust and biomass episodes

C. Shi et al.

Title Page

Abstract

Introduction

Conclusions

References

Tables

Figures

◀

▶

◀

▶

Back

Close

Full Screen / Esc

Printer-friendly Version

Interactive Discussion



Aerosol optical properties during dust and biomass episodes

C. Shi et al.

Title Page

Abstract

Introduction

Conclusions

References

Tables

Figures

◀

▶

◀

▶

Back

Close

Full Screen / Esc

Printer-friendly Version

Interactive Discussion



that less fraction of potassium and BC in aged particles, especially in smoldering combustion. Meanwhile, aged smoke presented more microphysical and chemical properties related to secondary aerosol, such as sulfate with scattering capability increased (Reid et al., 1998). Additionally, the hydrophilic particles in high number density were found to be more featured with light scattering (He et al., 2012a). Furthermore, due to the coastal location of our observation site, water-soluble and sea-salt aerosol frequently transported to Shanghai from the East China Sea and the Yellow Sea. These types aerosols can be mixed with the smoke and resulted in ascending SSA (Koepke et al., 1997; Dubovik et al., 2002; Kim et al., 2001).

3.5 Asymmetry factor (g)

Up to now, ground-based retrievals of asymmetry factor were rarely done in Shanghai. The ASY is inversed as the first moment of scattering phase function and biases a fundamental parameter in radiation transfer equation (Dubovik et al., 2002; Andrews et al., 2006). According to the basic definition, ASY is calculated intensity-weighted mean cosine of scattering angle (see in Sect. 2.2). Unity is regarded as a purely forward scattering indicator while zero represents aerosol symmetric scattering (Bergstrom et al., 2003). Various uncertainties existed in this parameter during the inversion as the vague determination of aerosol types (Dubovik and King, 2000). To minimize the uncertainty, the authors depicted averages of ASY at four wavelengths belonging to 50 daily samples (10 in episode condition) in Fig. 11. The g showed a decreasing trend at 440–870 nm and then increased weakly in NIR band for dust aerosol. On the other hand, g demonstrated a quasi-linear descending relationship at all observed wavelengths for biomass smoke aerosol, denoting its remarkable diversity of forward scattering capability in visible and NIR band. In general, the asymmetry factors in visible band were about 0.688, 0.693, 0.708 for dust, biomass days and normal days in Shanghai. This phenomenon in our observation highlighted the forward scattering caused by fine particles including biomass smoke and urban aerosol, which may exert warming effects in ground level to some extent. In dusty weather, it revealed the enhancement of the

Aerosol optical properties during dust and biomass episodes

C. Shi et al.

Title Page

Abstract

Introduction

Conclusions

References

Tables

Figures

◀

▶

◀

▶

Back

Close

Full Screen / Esc

Printer-friendly Version

Interactive Discussion



- Hess, M., Koepke, P., and Schult, I.: Optical properties of aerosols and clouds: the software package OPAC, *B. Am. Meteorol. Soc.*, 79, 831–844, 1998.
- Holben, B., Setzer, A., Eck, T., Pereira, A., and Slutsker, I.: Effect of dry-season biomass burning on Amazon basin aerosol concentrations and optical properties, 1992–1994, *J. Geophys. Res.*, 101, 19465–19481, 1996.
- Huang, C., Chen, C. H., Li, L., Cheng, Z., Wang, H. L., Huang, H. Y., Streets, D. G., Wang, Y. J., Zhang, G. F., and Chen, Y. R.: Emission inventory of anthropogenic air pollutants and VOC species in the Yangtze River Delta region, China, *Atmos. Chem. Phys.*, 11, 4105–4120, doi:10.5194/acp-11-4105-2011, 2011.
- Huang, K., Zhuang, G., Lin, Y., Li, J., Sun, Y., Zhang, W., and Fu, J. S.: Relation between optical and chemical properties of dust aerosol over Beijing, China, *J. Geophys. Res.*, 115, D00K16, doi:10.1029/2003JD003550, 2010.
- Huang, Y., Li, L., Li, J., Wang, X., Chen, H., Chen, J., Yang, X., Gross, D. S., Wang, H., Qiao, L., and Chen, C.: A case study of the highly time-resolved evolution of aerosol chemical and optical properties in urban Shanghai, China, *Atmos. Chem. Phys.*, 13, 3931–3944, doi:10.5194/acp-13-3931-2013, 2013.
- Jacobson, M. Z.: Strong radiative heating due to the mixing state of black carbon in atmospheric aerosols, *Nature*, 409, 695–697, 2001.
- Jinhuan, Q. and Liquean, Y.: Variation characteristics of atmospheric aerosol optical depths and visibility in North China during 1980–1994, *Atmos. Environ.*, 34, 603–609, 2000.
- Kaufman, Y., Tanré, D., Dubovik, O., Karnieli, A., and Remer, L.: Absorption of sunlight by dust as inferred from satellite and ground-based remote sensing, *Geophys. Res. Lett.*, 28, 1479–1482, 2001.
- Kim, D. H., Sohn, B. J., Nakajima, T., Takamura, T., Takemura, T., Choi, B. C., and Yoon, S. C.: Aerosol optical properties over East Asia determined from ground-based sky radiation measurements, *J. Geophys. Res.*, 109, D02209, doi:10.1029/2003JD003387, 2004.
- Kim, J., Yoon, S.-C., Jefferson, A., and Kim, S.-W.: Aerosol hygroscopic properties during Asian dust, pollution, and biomass burning episodes at Gosan, Korea in April 2001, *Atmos. Environ.*, 40, 1550–1560, 2006.
- King, M. D., Byrne, D. M., Herman, B. M., and Reagan, J. A.: Aerosol size distributions obtained by inversions of spectral optical depth measurements, *J. Atmos. Sci.*, 35, 2153–2167, 1978.
- Köpke, P., Hess, M., Schult, I., and Shettle, E.: Global Aerosol Data Set, Max-Planck-Institut für Meteorologie, Hamburg, Germany, 1997.

Aerosol optical properties during dust and biomass episodes

C. Shi et al.

Title Page

Abstract

Introduction

Conclusions

References

Tables

Figures

◀

▶

◀

▶

Back

Close

Full Screen / Esc

Printer-friendly Version

Interactive Discussion

- Kotchenruther, R. A. and Hobbs, P. V.: Humidification factors of aerosols from biomass burning in Brazil, *J. Geophys. Res.-Atmos.*, 103, 32081–32089, 1998.
- Lei, Y., Zhang, Q., He, K. B., and Streets, D. G.: Primary anthropogenic aerosol emission trends for China, 1990–2005, *Atmos. Chem. Phys.*, 11, 931–954, doi:10.5194/acp-11-931-2011, 2011.
- Levy, R. C., Remer, L. A., and Dubovik, O.: Global aerosol optical properties and application to Moderate Resolution Imaging Spectroradiometer aerosol retrieval over land, *J. Geophys. Res.*, 112, D13210, doi:10.1029/2006JD007815, 2007.
- Li, H., Han, Z., Cheng, T., Du, H., Kong, L., Chen, J., Zhang, R., and Wang, W.: Agricultural fire impacts on the air quality of Shanghai during summer harvesttime, *Aerosol and Air Quality Research*, 10, 95–101, 2010.
- Li, Z., Goloub, P., Devaux, C., Gu, X., Qiao, Y., Zhao, F., and Chen, H.: Aerosol polarized phase function and single-scattering albedo retrieved from ground-based measurements, *Atmos. Res.*, 71, 233–241, 2004.
- Li, Z., Chen, H., Cribb, M., Dickerson, R., Holben, B., Li, C., Lu, D., Luo, Y., Maring, H., and Shi, G.: Preface to special section on East Asian Studies of Tropospheric Aerosols: An International Regional Experiment (EAST-AIRE). *J. Geophys. Res.*, 112, D22S00, doi:10.1029/2007JD008479, 2007a.
- Limbeck, A., Kulmala, M., and Puxbaum, H.: Secondary organic aerosol formation in the atmosphere via heterogeneous reaction of gaseous isoprene on acidic particles, *Geophys. Res. Lett.*, 30, 1996, doi:10.1029/2003GL017738, 2003.
- Lu, Z., Zhang, Q., and Streets, D. G.: Sulfur dioxide and primary carbonaceous aerosol emissions in China and India, 1996–2010, *Atmos. Chem. Phys.*, 11, 9839–9864, doi:10.5194/acp-11-9839-2011, 2011.
- Martins, J. V., Artaxo, P., Liousse, C., Reid, J. S., Hobbs, P. V., and Kaufman, Y. J.: Effects of black carbon content, particle size, and mixing on light absorption by aerosols from biomass burning in Brazil, *J. Geophys. Res.*, 103, 32041–32050, 1998.
- Metz, B., Davidson, O., Bosch, P., Dave, R., and Meyer, L.: IPCC: Climate Change 2007: Mitigation, Contribution of Working Group III to the Fourth Assessment Report of the Intergovernmental Panel on Climate Change, Cambridge University Press, Cambridge, UK and New York, NY, USA, 2007.

Aerosol optical properties during dust and biomass episodes

C. Shi et al.

Title Page

Abstract

Introduction

Conclusions

References

Tables

Figures

◀

▶

◀

▶

Back

Close

Full Screen / Esc

Printer-friendly Version

Interactive Discussion

ing the Puerto Rico Dust Experiment (PRIDE), *J. Geophys. Res.-Atmos.*, 108, 8586, doi:10.1029/2002JD002493, 2003.

Reid, J. S., Koppmann, R., Eck, T. F., and Eleuterio, D. P.: A review of biomass burning emissions part II: intensive physical properties of biomass burning particles, *Atmos. Chem. Phys.*, 5, 799–825, doi:10.5194/acp-5-799-2005, 2005.

Remer, L. A., Kaufman, Y., Tanré, D., Mattoo, S., Chu, D., Martins, J., Li, R.-R., Ichoku, C., Levy, R., and Kleidman, R.: The MODIS aerosol algorithm, products, and validation, *J. Atmos. Sci.*, 62, 947–973, 2005.

Russell, P. B., Hobbs, P. V., and Stowe, L. L.: Aerosol properties and radiative effects in the United States east coast haze plume: An overview of the Tropospheric Aerosol Radiative Forcing Observational Experiment (TARFOX), *J. Geophys. Res.*, 104, 2213–2222, 1999.

Shindell, D. and Faluvegi, G.: Climate response to regional radiative forcing during the twentieth century, *Nat. Geosci.*, 2, 294–300, 2009.

Singh, R., Dey, S., Tripathi, S., Tare, V., and Holben, B.: Variability of aerosol parameters over Kanpur, northern India. *J. Geophys. Res.-Atmos.*, 109, D23206, doi:10.1029/2004JD004966, 2004.

Takemura, T., Nakajima, T., Dubovik, O., Holben, B. N., and Kinne, S.: Single-scattering albedo and radiative forcing of various aerosol species with a global three-dimensional model, *J. Climate*, 15, 333–352, 2002.

Takemura, T., Nozawa, T., Emori, S., Nakajima, T. Y., and Nakajima, T.: Simulation of climate response to aerosol direct and indirect effects with aerosol transport-radiation model, *J. Geophys. Res.-Atmos.*, 110, D02202, doi:10.1029/2004JD005029, 2005.

Wang, J., Guo, P., Li, X., Zhu, J., Reinert, T., Heitmann, J., Spemann, D., Vogt, J., Flaggmeyer, R.-H., and Butz, T.: Source identification of lead pollution in the atmosphere of Shanghai City by analyzing single aerosol particles (SAP), *Environ. Sci. Technol.*, 34, 1900–1905, 2000.

Wang, S., Zhou, B., Wang, Z., Yang, S., Hao, N., Valks, P., Trautmann, T., and Chen, L.: Remote sensing of NO₂ emission from the central urban area of Shanghai (China) using the mobile DOAS technique, *J. Geophys. Res.-Atmos.*, 117, D13305, doi:10.1029/2011JD016983, 2012.

Wang, X., Zhang, Y., Chen, H., Yang, X., Chen, J., and Geng, F.: Particulate nitrate formation in a highly polluted urban area: A case study by single-particle mass spectrometry in Shanghai, *Environ. Sci. Technol.*, 43, 3061–3066, 2009.

Aerosol optical properties during dust and biomass episodes

C. Shi et al.

Title Page

Abstract

Introduction

Conclusions

References

Tables

Figures

◀

▶

◀

▶

Back

Close

Full Screen / Esc

Printer-friendly Version

Interactive Discussion

- Wang, Y., Zhuang, G., Zhang, X., Huang, K., Xu, C., Tang, A., Chen, J., and An, Z.: The ion chemistry, seasonal cycle, and sources of $PM_{2.5}$ and TSP aerosol in Shanghai, *Atmos. Environ.*, 40, 2935–2952, 2006.
- Westerdahl, D., Wang, X., Pan, X., and Zhang, K. M.: Characterization of on-road vehicle emission factors and microenvironmental air quality in Beijing, China, *Atmos. Environ.*, 43, 697–705, 2009.
- Xia, X., Li, Z., Holben, B., Wang, P., Eck, T., Chen, H., Cribb, M., and Zhao, Y.: Aerosol optical properties and radiative effects in the Yangtze Delta region of China, *J. Geophys. Res.*, 112, D22S12, doi:10.1029/2007JD008859, 2007.
- Xin, J., Wang, S., Wang, Y., Yuan, J., Zhang, W., and Sun, Y.: Optical properties and size distribution of dust aerosols over the Tengger Desert in Northern China, *Atmos. Environ.*, 39, 5971–5978, 2005.
- Xu, J., Bergin, M., Yu, X., Liu, G., Zhao, J., Carrico, C., and Baumann, K.: Measurement of aerosol chemical, physical and radiative properties in the Yangtze delta region of China, *Atmos. Environ.*, 36, 161–173, 2002.
- Xue, Y., Xu, H., Li, Y., Yang, L., Mei, L., Guang, J., Hou, T., He, X., Dong, J., Chen, Z., and Qi, Y.: Long-term aerosol optical depth datasets over China retrieved from satellite data, *Atmos. Meas. Tech. Discuss.*, 4, 6643–6678, doi:10.5194/amtd-4-6643-2011, 2011.
- Ye, B., Ji, X., Yang, H., Yao, X., Chan, C. K., Cadle, S. H., Chan, T., and Mulawa, P. A.: Concentration and chemical composition of $PM_{2.5}$ in Shanghai for a 1-year period, *Atmos. Environ.*, 37, 499–510, 2003.
- Yu, X., Cheng, T., Chen, J., and Liu, Y.: A comparison of dust properties between China continent and Korea, Japan in East Asia, *Atmos. Environ.*, 40, 5787–5797, 2006.
- Yu, X., Shi, C., Ma, J., Zhu, B., Li, M., Wang, J., Yang, S., and Kang, N.: Aerosol optical properties during firework, biomass burning and dust episodes in Beijing, *Atmos. Environ.*, 81, 475–484, doi:10.1016/j.atmosenv.2013.08.067, 2013.
- Zhang, T., Cao, J., Tie, X., Shen, Z., Liu, S., Ding, H., Han, Y., Wang, G., Ho, K., and Qiang, J.: Water-soluble ions in atmospheric aerosols measured in Xi'an, China: Seasonal variations and sources, *Atmos. Res.*, 102, 110–119, 2011.

Aerosol optical properties during dust and biomass episodes

C. Shi et al.

Title Page

Abstract

Introduction

Conclusions

References

Tables

Figures

◀

▶

◀

▶

Back

Close

Full Screen / Esc

Printer-friendly Version

Interactive Discussion



Table 1. Number of validated sample^a s in the observation period since 28 March to 25 June.

Month	Mar	Apr	May	Jun	Total
Samples	4	22	15	9	50

^a CE318 ceased to observe in rainy days.

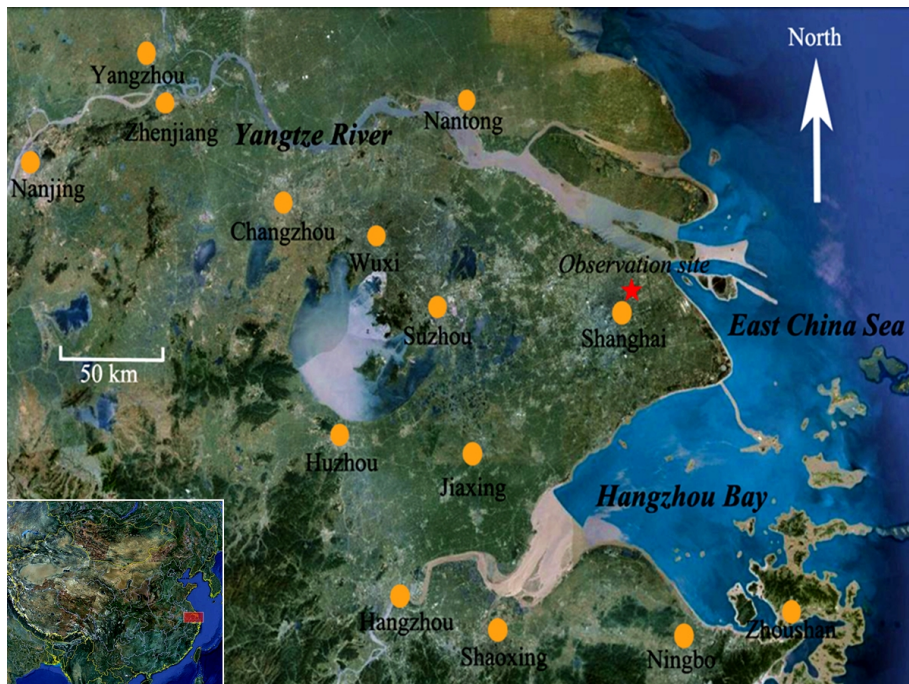


Fig. 1. Geographical location of observation site at Fudan University located in Shanghai from Google Earth.

Aerosol optical properties during dust and biomass episodes

C. Shi et al.

Title Page	
Abstract	Introduction
Conclusions	References
Tables	Figures
◀	▶
◀	▶
Back	Close
Full Screen / Esc	
Printer-friendly Version	
Interactive Discussion	



Aerosol optical properties during dust and biomass episodes

C. Shi et al.

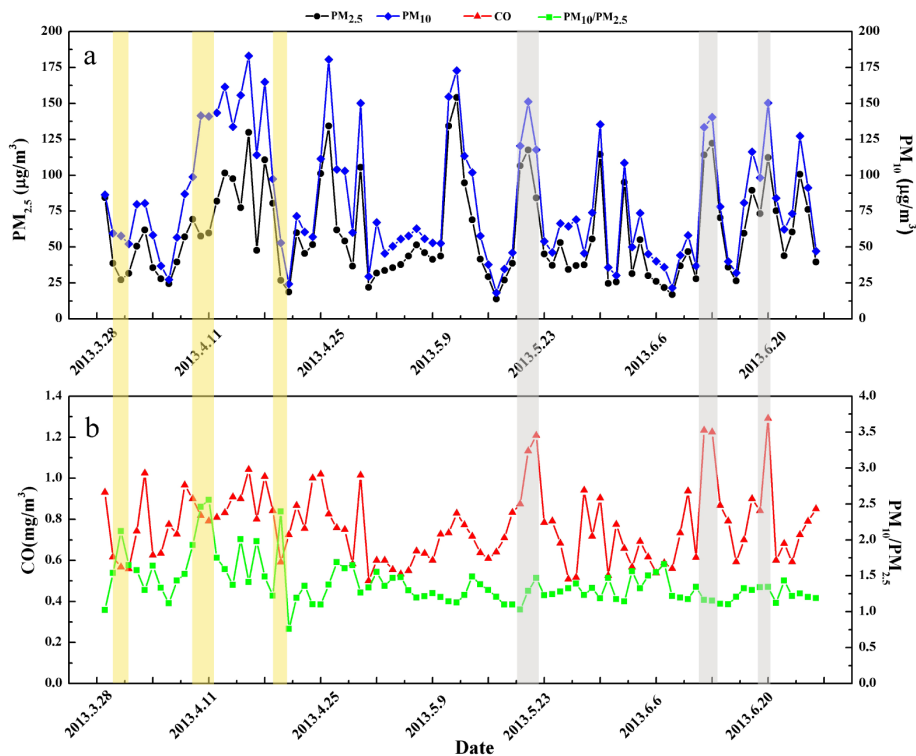


Fig. 2. Temporal variations of (a) daily-averaged mass concentrations of PM_{10} , $PM_{2.5}$ and (b) daily-averaged mass concentrations of CO, ratios between PM_{10} , $PM_{2.5}$ in observation period from 28 March to 25 June. Five dust days were in brown shadow while five biomass burning days were grey-shadowed.

Aerosol optical properties during dust and biomass episodes

C. Shi et al.

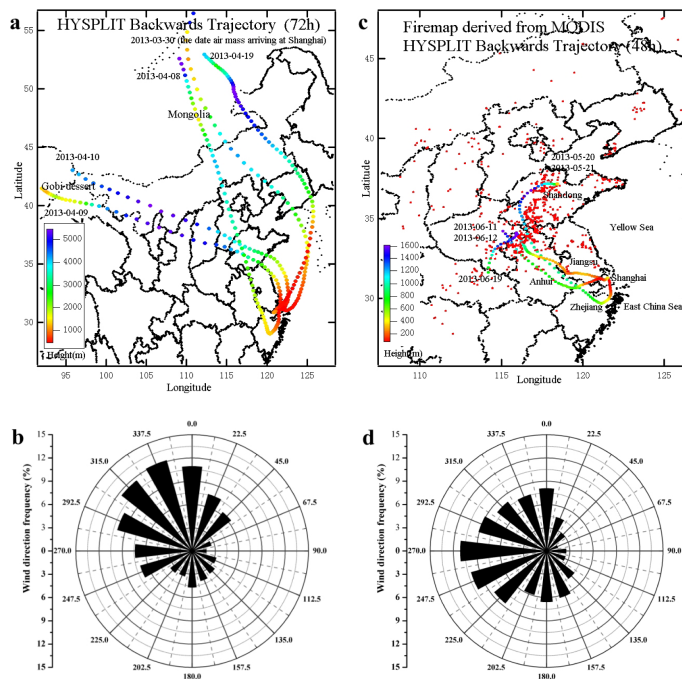


Fig. 3. Backward trajectories based on HYSPLIT model and firemaps derived from MODIS with wind roses during observation period. **(a)** Hourly resolved 72 h air mass back trajectories during dust episodes (five days); **(b)** wind roses during five dust days using hourly-averaged data for analysis; **(c)** hourly resolved 48 h air mass trajectory with daily firepots derived from MODIS during biomass burning episode (five days); **(d)** Wind roses during five biomass burning days using hourly-averaged data for analysis.

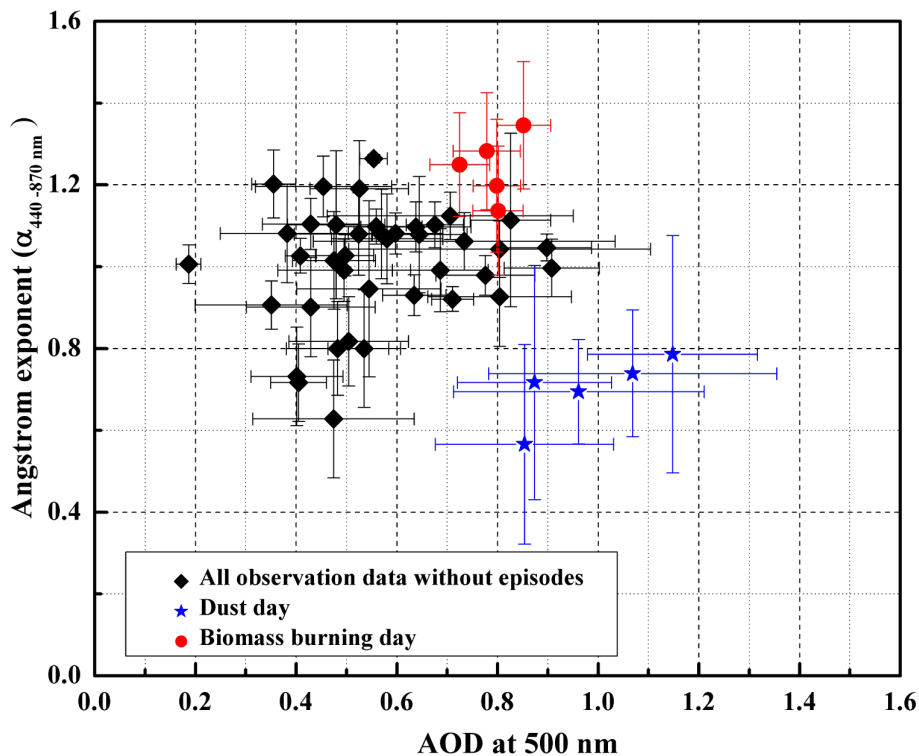


Fig. 5. Scatterplot of daily-averaged AOD at 500 nm and Ångström exponent in the observation period over Shanghai. The averages with standard deviation were calculated from all inversed AOD and Ångström exponent in each observation day. Five samples were for dust (in blue) and five samples were for biomass (in red) while forty samples represented normal condition (in black).

Aerosol optical properties during dust and biomass episodes

C. Shi et al.

Title Page	
Abstract	Introduction
Conclusions	References
Tables	Figures
◀	▶
◀	▶
Back	Close
Full Screen / Esc	
Printer-friendly Version	
Interactive Discussion	



Aerosol optical properties during dust and biomass burning episodes

C. Shi et al.

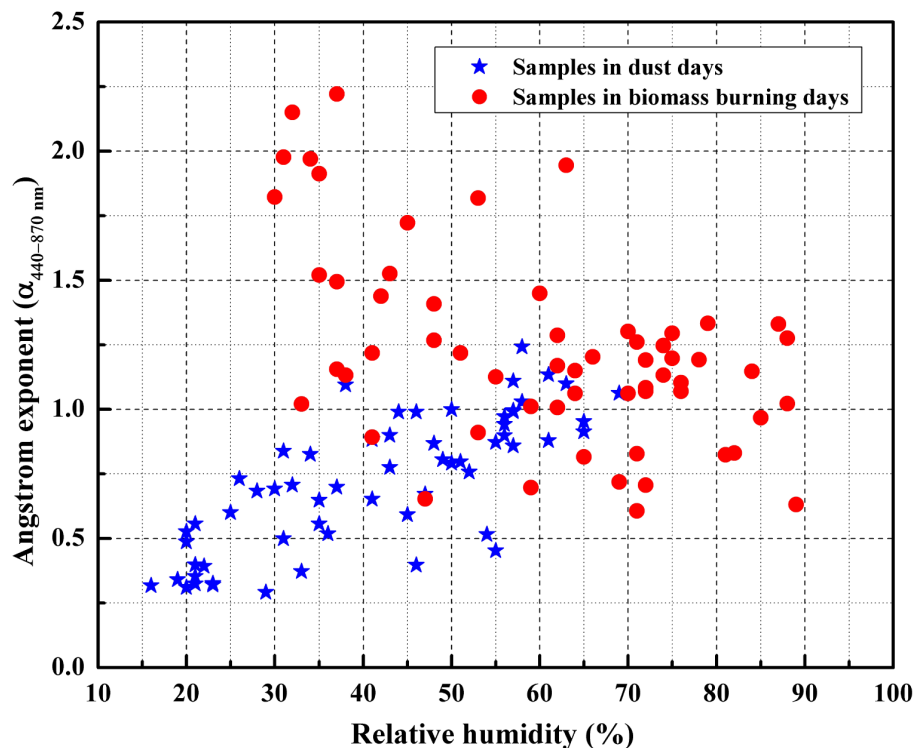


Fig. 6. Scatterplot of hourly-averaged relative humidity and Ångström exponent in dust (in blue) and biomass burning (in red) days over Shanghai. The data for each episode was based on hourly-averaged samples from 7 a.m. to 6 p.m. in every day, 60 × 2 samples in total.

[Title Page](#)[Abstract](#)[Introduction](#)[Conclusions](#)[References](#)[Tables](#)[Figures](#)[◀](#)[▶](#)[◀](#)[▶](#)[Back](#)[Close](#)[Full Screen / Esc](#)[Printer-friendly Version](#)[Interactive Discussion](#)

Aerosol optical properties during dust and biomass episodes

C. Shi et al.

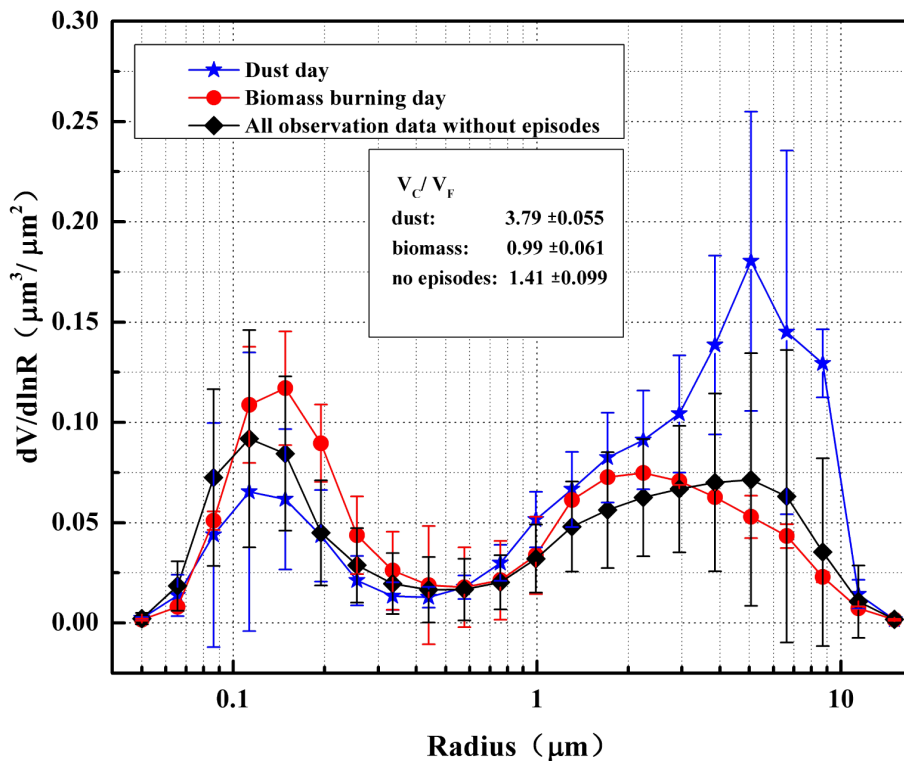


Fig. 7. Average aerosol volume size distribution with standard deviation in the observation period over Shanghai. The averages and deviations were calculated from each inversed volume concentration in 22 radius during five dust days (in blue), five biomass burning days (in red) and forty normal days (in black).

Title Page

Abstract

Introduction

Conclusions

References

Tables

Figures

◀

▶

◀

▶

Back

Close

Full Screen / Esc

Printer-friendly Version

Interactive Discussion

Aerosol optical properties during dust and biomass episodes

C. Shi et al.

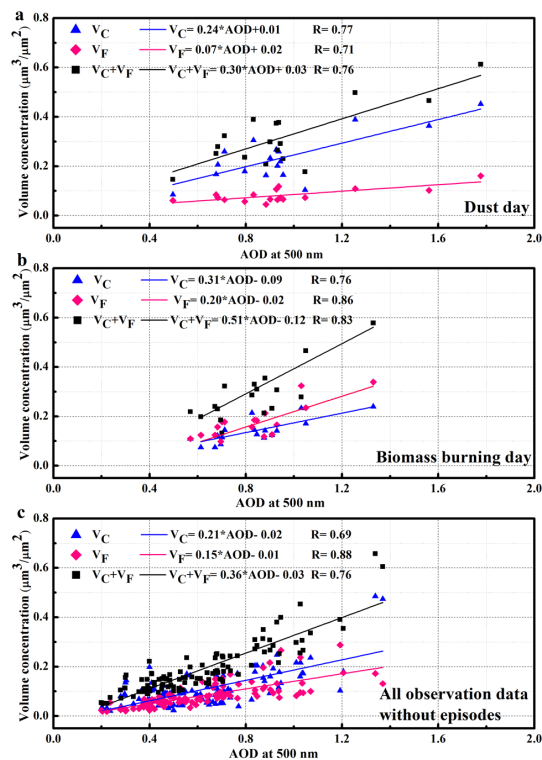


Fig. 8. The scatter-plot of aerosol volume concentration in the accumulation mode and coarse mode with AOD at 500 nm in **(a)** dust days; **(b)** biomass burning days; and **(c)** days without episodes over Shanghai. The blue line is the fitting line of the coarse mode aerosol volume concentration with AOD while the pink line is the fitting line of accumulation mode aerosol volume concentration with AOD, and the black line is the fitting line of the sum of the volume concentration of these two aerosol types with AOD.

Aerosol optical properties during dust and biomass episodes

C. Shi et al.

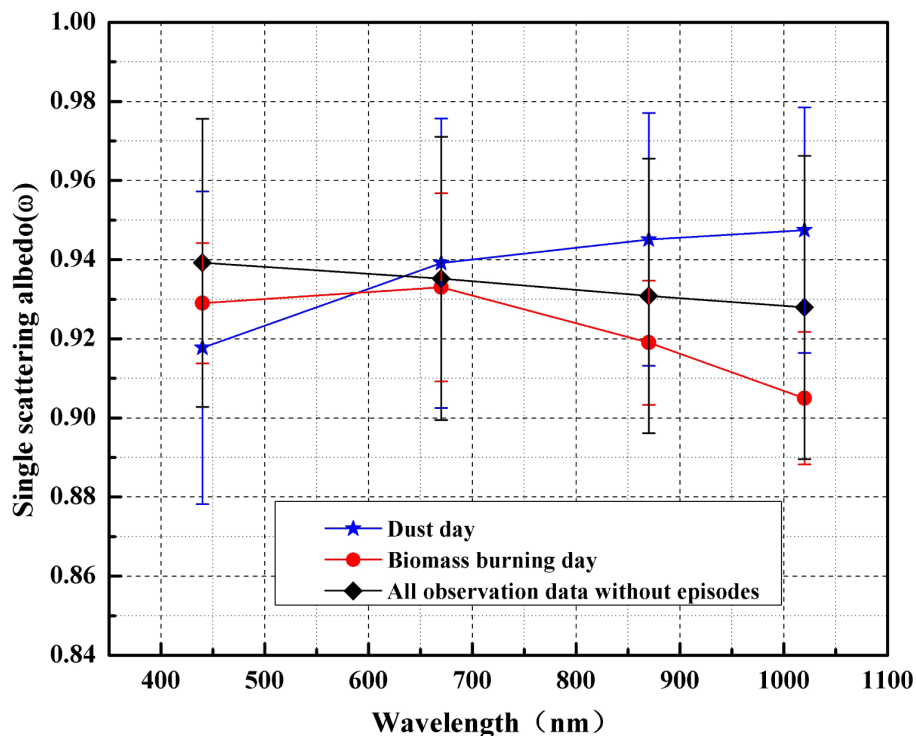


Fig. 9. Average aerosol single scattering albedo at 440, 675, 870 and 1020 nm with standard deviation in the observation period over Shanghai. The averages and deviations were calculated from each inversed SSA during five dust days (in blue), five biomass burning days (in red) and forty normal days (in black).

[Title Page](#)[Abstract](#)[Introduction](#)[Conclusions](#)[References](#)[Tables](#)[Figures](#)[◀](#)[▶](#)[◀](#)[▶](#)[Back](#)[Close](#)[Full Screen / Esc](#)[Printer-friendly Version](#)[Interactive Discussion](#)

Aerosol optical properties during dust and biomass episodes

C. Shi et al.

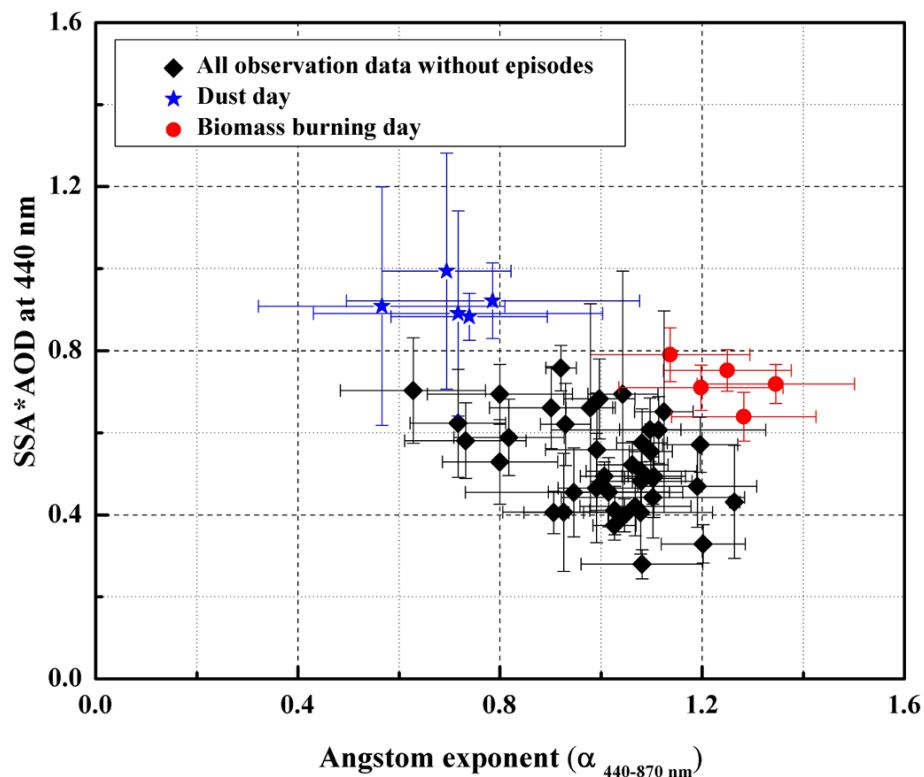


Fig. 10. Scatterplot of daily-averaged Ångström exponent and scattering coefficient (AOD · SSA) at 440 nm in the observation period over Shanghai. The averages with standard deviation were calculated from all inversed AOD, SSA and Ångström exponent in each observation day. Five samples were for dust (in blue) and five samples were for biomass (in red) while forty samples represented normal condition (in black).

Aerosol optical properties during dust and biomass episodes

C. Shi et al.

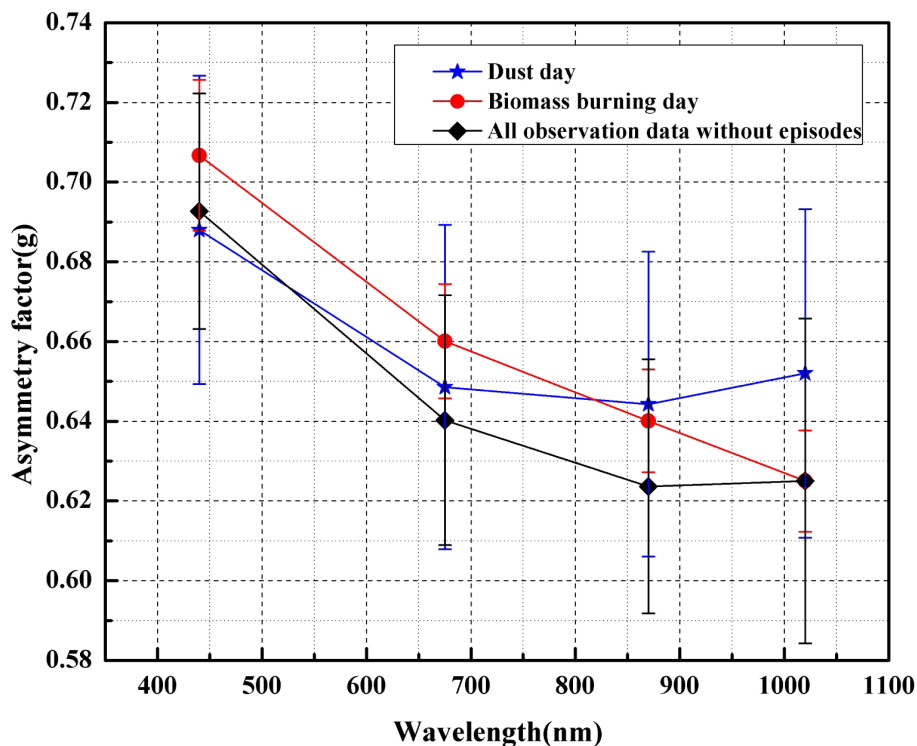


Fig. 11. Average aerosol asymmetry factor at 440, 675, 870 and 1020 nm with standard deviation in the observation period over Shanghai. The averages and deviations were calculated from each inversed ASY during five dust days (in blue), five biomass burning days (in red) and forty normal days (in black).

Aerosol optical properties during dust and biomass episodes

C. Shi et al.

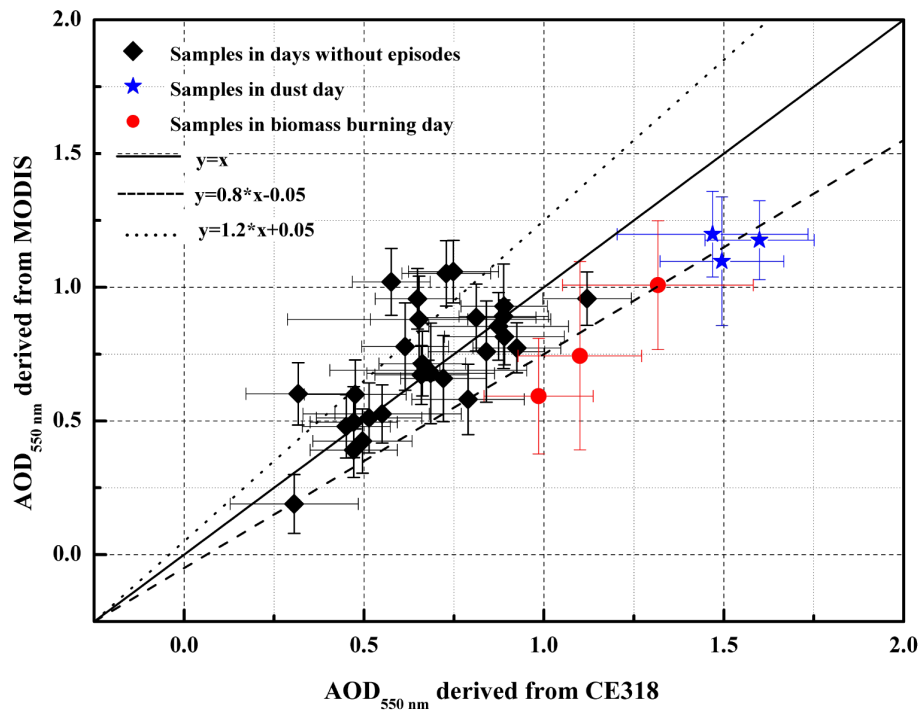


Fig. 12. Scatterplot of daily-averaged AOD at 550 nm derived from MODIS (C051 products) and CE318 in the observation period over Shanghai. There were 41 available samples in total (three for dust and three as biomass samples). The spatial averages with standard deviations of MODIS AOD were calculated in the range of 40km × 40km. AOD with its error bars from CE318 were temporal averages within ±30 min when satellite passed and averaged between AOD at 440 and 670 nm.

Title Page

Abstract

Introduction

Conclusions

References

Tables

Figures

◀

▶

◀

▶

Back

Close

Full Screen / Esc

Printer-friendly Version

Interactive Discussion